Vessel Network Architecture of Adult Human Islets Promotes Distinct Cell-Cell Interactions *In Situ* and Is Altered After Transplantation

Christian M. Cohrs,[1,2,3]* Chunguang Chen,[1,2,3]* Stephan R. Jahn,[1,2,3] Julia Stertmann,[1,2,3] Helena Chmelova,[1,2,3] Jürgen Weitz,[4] Andrea Bähr,[7] Nikolai Klymiuk,[7] Anja Steffen,[1,2,5] Barbara Ludwig,[1,2,5] Virginia Kamvissi,[5,8] Eckhard Wolf,[2,7] Stefan R. Bornstein,[1,2,5,8] Michele Solimena,[1,2,6] and Stephan Speier[1,2,3]

[1]Paul Langerhans Institute Dresden of Helmholtz Zentrum München at the University Clinic Carl Gustav Carus of Technische Universität Dresden, Helmholtz Zentrum München, 85764 München-Neuherberg, Germany; [2]German Center for Diabetes Research, 85764 München-Neuherberg, Germany; [3]DFG-Center for Regenerative Therapies Dresden, Faculty of Medicine, University Clinic Carl Gustav Carus, Technische Universität Dresden, 01307 Dresden, Germany; [4]Department of GI, Thoracic and Vascular Surgery, University Clinic Carl Gustav Carus, Technische Universität Dresden, 01307 Dresden, Germany; [5]Department of Medicine III, University Clinic Carl Gustav Carus, Technische Universität Dresden, 01307 Dresden, Germany; [6]Max Planck Institute of Molecular Cell Biology and Genetics, 01307 Dresden, Germany; [7]Institute of Molecular Animal Breeding and Biotechnology, Ludwig-Maximilians-Universität München, 81377 Oberschleißheim, Germany; and [8]Division of Diabetes and Nutritional Sciences, King's College London, SE19NH London, United Kingdom

Islet-cell hormone release is modulated by signals from endothelial and endocrine cells within the islet. However, models of intraislet vascularization and paracrine cell signaling are mostly based on the rodent pancreas. We assessed the architecture and endocrine cell interaction of the vascular network in unperturbed human islets *in situ* and their potential to re-establish their endogenous vascular network after transplantation *in vivo*. We prepared slices of fresh pancreas tissue obtained from nondiabetic patients undergoing partial pancreatectomy. In addition, we transplanted human donor islets into the anterior chamber of the mouse eye. Next, we performed three-dimensional *in situ* and *in vivo* imaging of islet cell and vessel architecture at cellular resolution and compared our findings with mouse and porcine islets. Our data reveal a significantly different vascular architecture with decreased vessel diameter, reduced vessel branching, and shortened total vessel network in human compared with mouse islets. Together with the distinct cellular arrangement in human islets, this limits β to endothelial cell interactions, facilitates connection of α and β cells, and promotes the formation of independent β-cell clusters within islets. Furthermore, our results show that the endogenous vascular network of islets is significantly altered after transplantation in a donor age-related mechanism. Thus, our study provides insight into the vascular architecture and cellular arrangement of human islets with apparent consequences for intercellular islet signaling. Moreover, our findings suggest that human islet engraftment after transplantation can be improved by using alternative, less mature islet-cell sources. **(*Endocrinology* 158: 1373–1385, 2017)**

Under physiological conditions, endocrine cell function in islets of Langerhans is modulated by various cellular interactions (1). This includes paracrine and juxtacrine crosstalk of endocrine cells (2–4), as well as signaling between endothelial and endocrine cells (5, 6). Hereby, islet vascularization not only allows direct

ISSN Print 0013-7227 ISSN Online 1945-7170
Printed in USA

Received 20 March 2016. Accepted 24 January 2017.
First Published Online 27 January 2017

*These authors contributed equally to this study.

Abbreviations: 3D, three-dimensional; AC, anterior chamber of the mouse eye; PBS, phosphate-buffered saline; SEM, standard error of the mean.

cellular modulation by endothelial cells but also facilitates paracrine regulation by directed blood flow through the islet (7). Therefore, vascular network characteristics and spatial arrangement of islet endocrine and endothelial cells will determine regulated hormone release in response to changing blood glucose levels.

Islet-cell composition and morphology differ among species (8–11), but the detailed spatial arrangement of human islet cells is still debated (11, 12). This is at least partially due to the use of thin histological sections, which limits conclusions on the spatial arrangements of cells. Furthermore, it prevents thorough investigations of the architecture of the intraislet vascular network. So far, three-dimensional (3D) analysis of human islet vascularization has been restricted to corrosion-cast studies lacking cellular compartments of the islet (13). Therefore, surprisingly little is known about the unperturbed 3D intraislet vascular network and its cellular interactions in human islets.

We assessed the 3D vascular network in combination with endocrine cell configuration of human islets in pancreatic tissue *in situ* (14). Our data reveal a different vascular architecture and low vascular fraction of human islets with smaller vessel diameter, reduced vessel branching, and shortened total vessel network in comparison with mouse islets. This contributes to a distinct 3D morphology with reduced β to endothelial cell contact, increased α–β cell interactions, and the formation of distinct β-cell clusters in human islets. Furthermore, our results show that the intraislet vascular network is dramatically altered after transplantation in a donor age-dependent manner, which has implications for therapeutic islet transplantation.

Design and Methods

Pancreas tissue samples and preparation of pancreas tissue slices

Pancreas tissue slices were prepared from 1-year and 12-week-old male and female B6.129S7-*Rag1*^{tm1Mom}/J (BL6 Rag$^{-/-}$) mice (n = 4 to 5 per group). Human tissue (Table 1) was obtained after partial pancreatectomy [n = 4; mean age ± standard error of the mean (SEM), 62.3 ± 4.9 years; mean body mass index ± SEM, 27.5 ± 2.2 kg/m^2; no history of diabetes] and informed consent was available from all patients. Porcine pancreatic tissue of pigs 6 to 9 months old was supplied by a local slaughterhouse. Tissue slices were prepared as previously described (14–16). Briefly, for mouse-tissue preparation, pancreata were injected with 1.25% low-melting-point agarose (Roth, Karlsruhe, Germany) after euthanizing the mouse. After solidification, the pancreas was excised and embedded in agarose (1.25%). Porcine tissue was infused with 1.25% agarose and embedded in 2% agarose. Human tissue was solely embedded with 3.8% agarose. Pancreas tissue slices were made at a thickness of 150 μm for mouse and porcine tissue and 120 μm for human tissue, using a semiautomated vibratome (Leica, Wetzlar, Germany). For every individual, a minimum of 5 islets were analyzed. All experiments were approved by the Committee on the Ethics of Animal Experiments of the State Directory of Saxony and the Ethics Committee of the Technische Universität Dresden.

Islet isolation and transplantation, and engraftment of islets in the anterior chamber of the eye

Mouse islet isolation of 1-year and 12-week-old mice was performed as previously reported (17). Human islets (tebu-bio, Le Perray En Yvelines, France) used for transplantation (Table 2) originated from 4 donors (mean age ± SEM, 30.8 ± 10.0 years; mean body mass index ± SEM, 22.4 ± 1.2 kg/m^2; no history of diabetes). After shipment, islets rested overnight in CMRL 1066 medium (Corning cellgro; Mediatech, Herndon, VA) supplemented with 2 g/L human serum albumin and 100 unit/mL penicillin/streptomycin prior to transplantation. Following a modified Ricordi method (18), porcine islets were isolated from 0.5-, 1.5-, 3-, and 5-year-old pigs and transplanted 3 to 4 days after isolation. Pancreatic islet transplantation into the anterior chamber of the mouse eye (AC) of NOD.CB17-*Prkdc*^{scid}/J mice was performed as described (17). Briefly, mice were anesthetized by inhalation of 2% isoflurane in 100% oxygen via a face mask. A 25-gauge needle was used to make a small incision in the cornea, close to the corneal limbus, and 20 to 25 islets in phosphate-buffered saline (PBS) were slowly injected into the AC, using a custom-made beveled glass cannula (outer diameter, 0.4 mm; inner diameter, 0.32 mm; Hilgenberg GmbH, Malsfeld, Germany). Islets were allowed to engraft for 8 weeks.

Immunohistochemistry

Pancreas tissue slices were stained as described (14) with antibodies to insulin (1:500; Dako; Agilent, Waldbronn, Germany) and glucagon (1:2000; Sigma Aldrich, Hamburg, Germany) visualized by Alexa Fluor 488, 633 secondary antibodies (1:200; Thermo Fisher Scientific, Darmstadt, Germany; Table 3). Briefly, after vibratome slicing, slices were fixed in 4% paraformaldehyde for 2 hours at 4°C. After a permeabilization step in PBS + 1% Triton-X for 2 hours and blocking for 1 hour with goat serum dilution buffer solution + 0.6% Triton-X, primary antibodies were applied in blocking solution and incubated overnight at 4°C. After washing, slices were incubated

Table 1. Information on Patients Who Underwent Partial Pancreatectomy for *In Situ* Analyses

Patient ID No.	Age, y	Sex	BMI, kg/m^2	Diabetic Status	Tumor	Tissue Origin
PPP1	74	Male	31.2	Nondiabetic	Acinic cell carcinoma of the pancreas	Pancreas head
PPP2	60	Male	23.2	Nondiabetic	Metastatic infiltration of a squamous cell carcinoma	Pancreas head
PPP3	66	Female	24.2	Nondiabetic	Serous oligocystic adenoma	Pancreas tail
PPP4	51	Male	31.4	Nondiabetic	Adenocarcinoma of *Ampulla Vateri*	Pancreas head

Abbreviations: BMI, body mass index; ID, identification; PPP, patient who underwent partial pancreatectomy.

Table 2. Information on Human Islet Donors for Transplantation Into the AC of Mice

ID No.	Age	Sex	BMI, kg/m^2	Diabetic Status
OD1	19	Male	19.0	No diabetes history
OD2	23	Male	23.8	No diabetes history
OD3	51	Female	24.4	No diabetes history
OD4	59	Male	22.4	No diabetes history

Abbreviations: BMI, body mass index; OD, organ donor.

with secondary antibodies and 4′,6-diamidino-2-phenylindole (2.5 mg/mL; Sigma-Aldrich, Hamburg, Germany) in blocking solution at 4°C overnight and then washed. Vessels were visualized by incubating stained slices with DyLight 594-labeled *Lycopersicon esculentum* (tomato) lectin (10 μg/mL; Vector Laboratories; Biozol, Munich, Germany) overnight at 4°C. Specificity of lectin labeling was assessed with an antibody to type IV collagen (1:200; Abcam, Cambridge, United Kingdom), a marker for the blood-vessel basement membrane in islets (19). These control stainings showed that all tubular structures within an islet were also labeled by lectin (Supplemental Fig. 1).

Imaging and analysis

In vivo imaging was conducted 8 weeks after transplantation, as described in detail (17, 20, 21). Briefly, mice were intubated (BioLite; Braintree Scientific, Inc., Braintree, MA) and anesthetized with 2% isoflurane in 100% oxygen with a 270-μL stroke volume at 250 strokes/min. Pupil dilation and iris movement were limited by a drop of 0.4% pilocarpine (Pilomann; Bausch & Lomb, Rochester, NY) in PBS placed on the cornea. For confocal and 2-photon imaging, an upright laser-scanning microscope (LSM780 NLO; Zeiss, Jena, Germany) equipped with a 2-photon laser (Chameleon Vision II; Coherent, Inc., Santa Clara, CA) and W Plan-Apochromat 320/1.0 differential interference contrast and M27 75-mm objective (Zeiss, Jena, Germany) was used. Total islet volume was assessed by backscatter laser light detected at 633 nm. Vessels were visualized by injecting 0.6 mg/mL fluorescein isothiocyanate-Dextran (Life Technologies; Thermo Fisher Scientific, Darmstadt, Germany) in PBS into the tail vein. Fluorescein isothiocyanate was excited by a two-photon laser at 930 nm and detected at 500 to 550 nm. For pancreas tissue slices, images were acquired solely by confocal imaging. The 4′,6-diamidino-2-phenylindole signal was excited at 405 nm and a detection range of 405 to 460 nm. Alexa Fluor 488 and 633 were excited at 488 and 633 nm, respectively, and detected at 490 to 540 nm and 640 to 720 nm, respectively. Lectin was excited at 561 nm and detected at 590 to 630 nm. *In vivo* imaging was performed at a single plain resolution of 512 × 512 pixels; *in situ* imaging was performed at a resolution of 1024 × 1024 pixels. Pixel size in x- and y-dimensions was between 0.555 and 3.02 μm, and z-stacks were acquired with a step size of 1.5 μm.

Three-dimensional analysis of *in vivo* and *in situ* images was performed using Imaris 8.1 (Bitplane AG, Zurich, Switzerland). Islet volume was calculated by surface rendering. Cellular and vascular fractions were quantified from median filtered images within the top 60 μm. Vessel network analysis was performed with the FilamentTracer plugin (*i.e.*, total vessel network length, number of branch points, mean segment length, vessel diameter). Normalization of branch points and vessel length was calculated by total branch points per islet volume analyzed times 10^3 and by total vessel length per islet volume analyzed times 10^3. Similar to a previous approach performed on histological thin sections (22, 23), we measured distances of endocrine cell nuclei in three dimensions. Endocrine cell nuclei were detected and quantified by the spot algorithm. Distances were calculated using the distance transformation plugin in 32-bit float images for spots to surfaces.

Statistical analyses and calculations

Data are presented as mean ± SEM and were compared by unpaired t tests or analysis of variance (Prism; GraphPad Software, San Diego, CA). Multiple comparisons were adjusted by Sidak correction, when necessary. Statistical significance was set at $P < 0.05$.

Results

Human islets exhibited a markedly different vascular network

We performed a detailed investigation of the 3D architecture of human islets, including the vascular network, endocrine cell composition, and cell-cell arrangement. Slices of freshly prepared pancreatic tissue obtained from nondiabetic patients undergoing partial pancreatectomy (Table 1) were compared with fresh mouse pancreas tissue slices from 1-year-old mice [Fig. 1(a) and 1(b)], thereby accounting for the mature age of human donors. The tissue-slice approach allowed analysis of unperturbed human and mouse islets within their intact pancreatic environment in 3 dimensions at subcellular resolution. Vessel network analysis revealed that mean vessel segment length, the distance between 2 branch points, was comparable between human and mouse islets [Fig. 1(c)], whereas the number of branch points was significantly lower in human islets [0.048 ± 0.005 vs 0.134 ± 0.017; Fig. 1(d)], depicting a less-complex vascular network in human islets. Furthermore, total vessel

Table 3. Antibodies Used in This Study and Their Targets

Peptide/Protein Target	Antibody	Manufacturer, Catalog No.	Species Raised in; Monoclonal or Polyclonal	Dilution
Insulin	Anti-insulin	Dako, A0564	Guinea pig; polyclonal	1:500
Glucagon	Anti-glucagon	Sigma-Aldrich, G2654	Mouse; monoclonal	1:1000
Collagen type IV	Anti-collagen IV	Abcam, ab19808	Rabbit; polyclonal	1:200

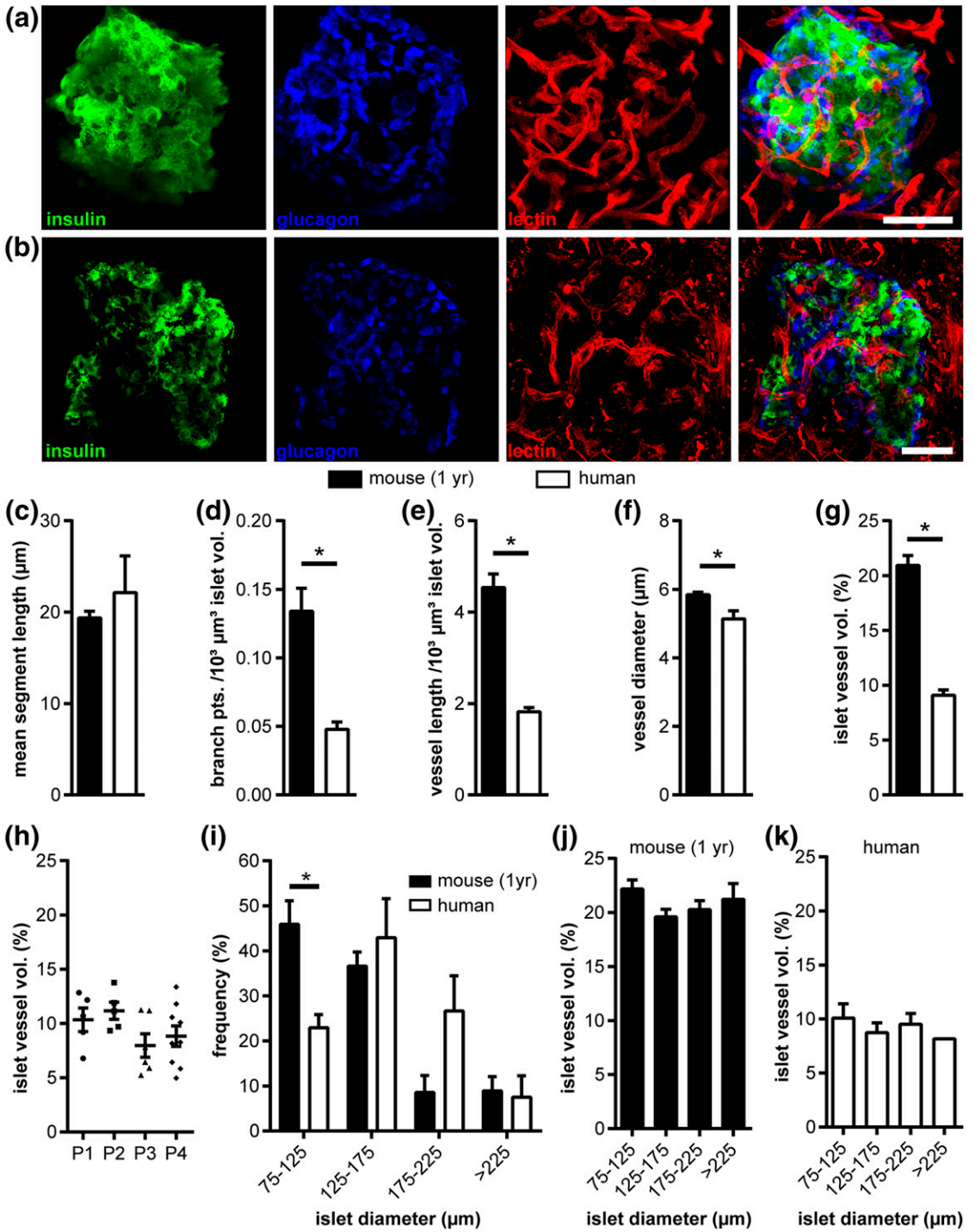

Figure 1. Vascular network of human and mouse islets *in situ*. (a,b) Fluorescence images of (a) a mouse and (b) a human islet within pancreas tissue slices. Images show maximum intensity projections (MIPs) of staining for insulin (green), glucagon (blue), and blood vessels (red), as well as a merged MIP. (c–k) *In situ* islet vessel network analysis of a 1-year-old mouse and adult human samples: (c) mean vessel segment length, (d) normalized number of branch points, (e) normalized vessel length, (f) mean vessel diameter, and (g) mean islet vessel volume fraction. (h) Islet vessel volume fraction of patients who underwent partial pancreatectomy. (i–k) Effect of islet size on vascular fraction: (i) distribution of human and mouse islet size in pancreas tissue slices, (j) vessel volume fractions for mouse, and (k) human islets grouped by islet size. Values are given as mean ± SEM for 10 mice (n = 97 islets; 9.7 ± 0.7 islets per mouse) and 4 humans (n = 25 islets; 6.25 ± 1.25 islets per donor). $*P < 0.05$. Scale bars = 50 µm. pts., points; vol., volume.

network length was shorter in human islets [1.82 ± 0.1 vs 4.54 ± 0.29 µm/10^3 µm^3 islet; Fig. 1(e)] and vessel diameter significantly smaller [5.1 ± 0.2 vs 5.8 ± 0.1 µm; Fig. 1(f)]. Altogether, this resulted in a substantially lower vascular component in human islets [9.1% ± 0.5% vs 20.9% ± 0.9%; Fig. 1(g)], which was consistent for the islets of all 4 patients analyzed [Fig. 1(h)]. Because mice showed a higher frequency of smaller islets *in situ*

compared with humans [Fig. 1(i)], we evaluated if the vascularization of islets was influenced by islet size. However, we did not observe any significant effect of islet size on islet vascular fraction in either species [Fig. 1(j) and 1(k); Supplemental Fig. 2)]. In addition, we did not detect any major sex-specific differences in mouse islet vascularization (Supplemental Fig. 3).

Vessel and endocrine cell architecture of human islets promoted distinct cell-cell interactions of α, β, and endothelial cells

Next, we investigated if the distinct vascular architecture within human islets has a consequence for the formation of endocrine-endothelial cell interactions. Endocrine cell composition of mouse islets in pancreas tissue slices showed the typical core-mantle structure and a significantly higher β-cell fraction compared with human [Fig. 2(a–c) and 2(g)]. In contrast, 3D assessment of human islet morphology demonstrated a well-defined arrangement of α cells throughout the entire islet, with α cells located preferentially along the blood vessels [Fig. 2(d–f) and 2(i)]. Detailed morphometric analysis revealed that the spatial arrangement of endocrine and endothelial cells differed between islets of the two species. In mouse islets, >90% of β and α cells were located next to a blood vessel [0- to 10-μm nucleus-to-vessel-surface distance; Fig. 2(h) and 2(i)]. In human islets, a significantly smaller fraction of both endocrine cell types was located directly next to an endothelial cell [60.7% ± 4.9% and 75.4% ± 4.2% of β and α cells, respectively, in a 0- to 10-μm nucleus-to-vessel-surface distance; Fig. 2(h) and 2(i)]. Consequently, in human islets, significantly more endocrine cell nuclei were found within 10 to 20 μm of the next blood vessel, reducing the chance of a direct contact with an endothelial cell [Fig. 2(h) and 2(i)]. Notably, 7.5% ± 1.9% and 5.2% ± 1.4% of human β- and α-cell nuclei were located even more than 20 μm away from the next blood vessel [Fig. 2(h) and 2(i)], essentially excluding any contact.

Paracrine interactions of different endocrine cell types within the islet were shown to modulate hormone release (1). Therefore, we assessed the relative location of α and β cells within islets in three dimensions. We found 51.0% ± 4.4% of mouse β cells located in immediate proximity to α cells [0- to 10-μm nucleus-to-cell-surface distance; Fig. 2(j)]. Another 24.4% ± 1.1% of mouse β-cell nuclei were near an α cell [10 to 20 μm; Fig. 2(j)], potentially enabling direct contact. However, nearly 25% of β-cell nuclei were located >20 μm away from the next α cell [Fig. 2(j)], making direct contact between the cells highly unlikely. In contrast, in human islets, almost all β cells were located immediately next (85.8% ± 1.7% in a 0- to 10-μm distance) or close (12.0% ± 0.8% in a 10- to 20-μm distance) to an α cell [Fig. 2(j)], and this layout was identical in all studied patient samples [Fig. 2(k)]. The difference in paracrine cell-cell arrangement was further corroborated by comparison of the neighboring cell configuration. Whereas mouse islets displayed equal portions of β cells with either only β cells or a mix of β and α cells as neighbors (50.9% ± 4.1% vs 46.1% ± 3.6%), in human islets, the vast majority of β cells (>80%) exhibited a mixed neighborhood of β and α cells [Fig. 2(l)]. Interestingly, the cellular surrounding of α cells in both species did not differ [Fig. 2(l)].

Finally, we evaluated if the interspersed arrangement of α and β cells led to a different grouping of β cells in human islets, by assessing the number of separate clusters of β cells within an islet. As expected from their general architecture, almost all mouse islets were composed of only 1 cluster of adjoining β cells [94.6% ± 3.2%; Fig. 2(m)]. In contrast, significantly less human islets (59.2% ± 3.5%) showed full connectivity of all β cells, whereas a substantial number of human islets were found to be composed of at least two β-cell clusters [Fig. 2(m)]. Thus, mouse and human islets displayed a markedly different cell-cell arrangement, affecting potential endocrine-endothelial and endocrine-endocrine cell communication.

Aged donor islets lacked the potential to rebuild their endogenous blood vessel network after transplantation

Islet transplantation is considered a promising therapeutic approach for diabetes and correct engraftment of islets after transplantation is crucial for its long-term success. To investigate whether mouse and human islets can rebuild the described specific endogenous vascular network after transplantation, we transplanted isolated mouse islets from 1-year-old donors and human islets obtained from organ donors (Table 2) into the AC of NOD.CB17-*Prkdc*^{scid}/J mice [Fig. 3(a) and 3(b)]. *In vivo* imaging 8 weeks after engraftment revealed that mouse islets showed the typical tortuous vascular network [Fig. 3(a)], whereas vessels within transplanted human islets were restricted mostly to the islet core [Fig. 3(b)], showing vastly different network parameters between human and mouse islets after transplantation into the same environment. Although mean segment length was similar [Fig. 3(c)], branch points [0.01 ± 0.001 vs 0.04 ± 0.001points per 10^3 μm^3 islet; Fig. 3(d)], total vessel network length [0.49 ± 0.04 vs 2.21 ± 0.09 μm/10^3 μm^3 islet; Fig. 3(e)], vessel diameter [6.4 ± 0.29 vs 7.68 ± 0.13 μm; Fig. 3(f)], and fractional vessel volume [3.1% ± 0.3% vs and 15.1% ± 0.29%; Fig. 3(g)] of transplanted human islets were substantially lower in comparison with mouse. To minimize an effect of islet size on revascularization in our study, mouse

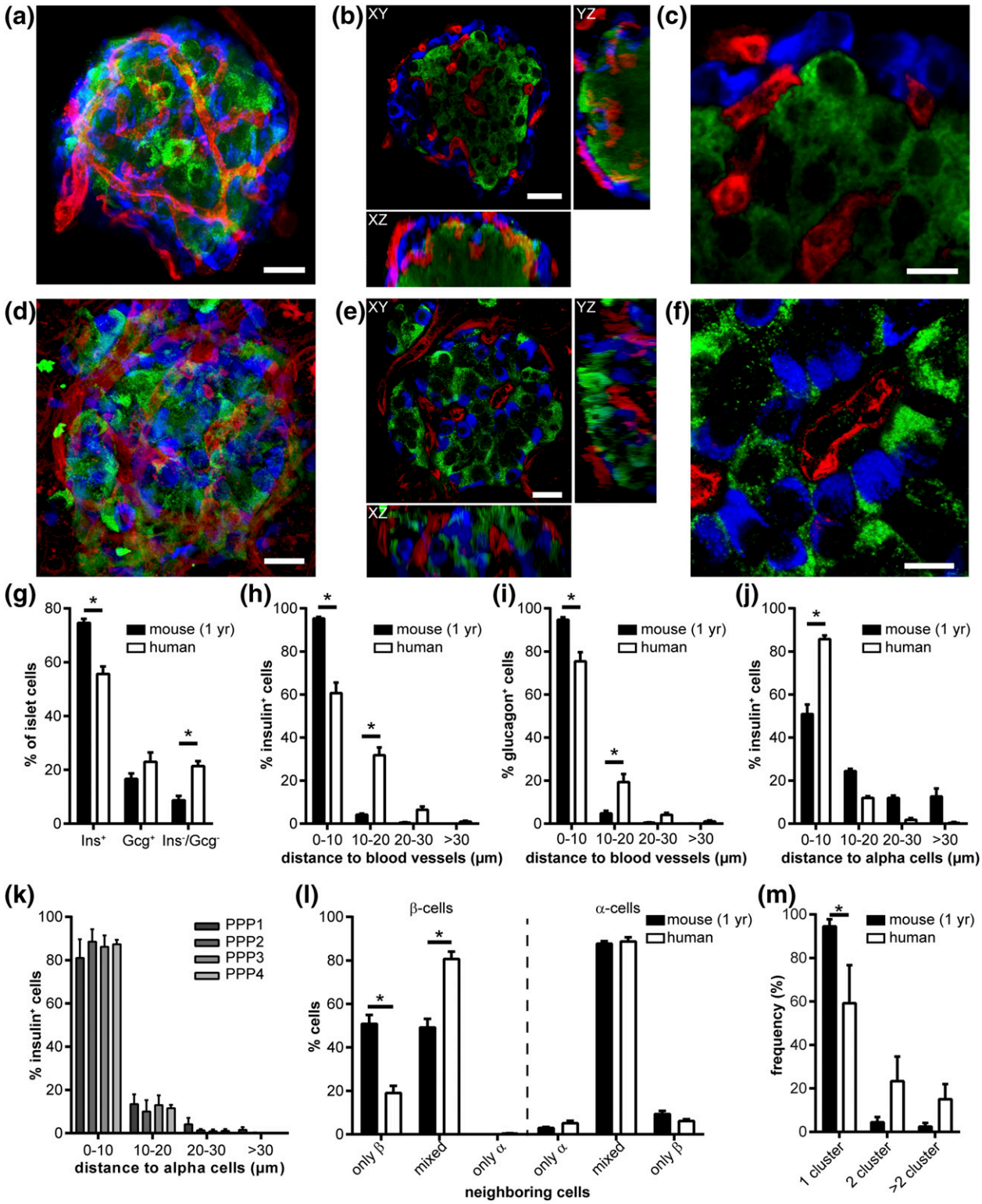

Figure 2. Spatial distribution of endocrine cells and vessels in adult human and 1-year-old mouse islets *in situ*. (a–f) Images of (a–c) a mouse and (d–f) human islet within pancreas tissue slices. Images show (a, d) an MIP; (b, e) optical sections within an islet in XY (top), YZ (right), and XZ (below); and (c, f) a magnified view of an optical section stained for insulin (green), glucagon (blue), and blood vessels (red). (g) Compositional analysis of Ins^+, Gcg^+, and Ins^-/Gcg^- cell volumes in mouse and human islets *in situ*. (h) Distribution of Ins^+ cell nuclei and (i) Gcg^+ cell nuclei minimum distance to blood-vessel surface in mouse and human islets *in situ*. (j) Distribution of Ins^+ cell nuclei minimum distance to Gcg^+ cell surface in mouse and human islets *in situ*. (k) Human Ins^+–Gcg^+ cell distances grouped by donor patient. (l) Distribution of neighboring cell configuration for Ins^+ cells and Gcg^+ cells in mouse and human islets *in situ*. (m) Frequency of cluster number within single islets of mouse and human islets *in situ*. Values are given as mean ± SEM for 10 mice (n = 97 islets; 9.7 ± 0.7 islets per mouse) and 4 humans (n = 25 islets; 6.25 ± 1.25 islets per donor). $*P < 0.05$. Scale bars = 20 µm (a,b,d,e) and 10 µm (c,f). Ins, insulin; Gcg, glucagon; PPP, patient who underwent partial pancreatectomy.

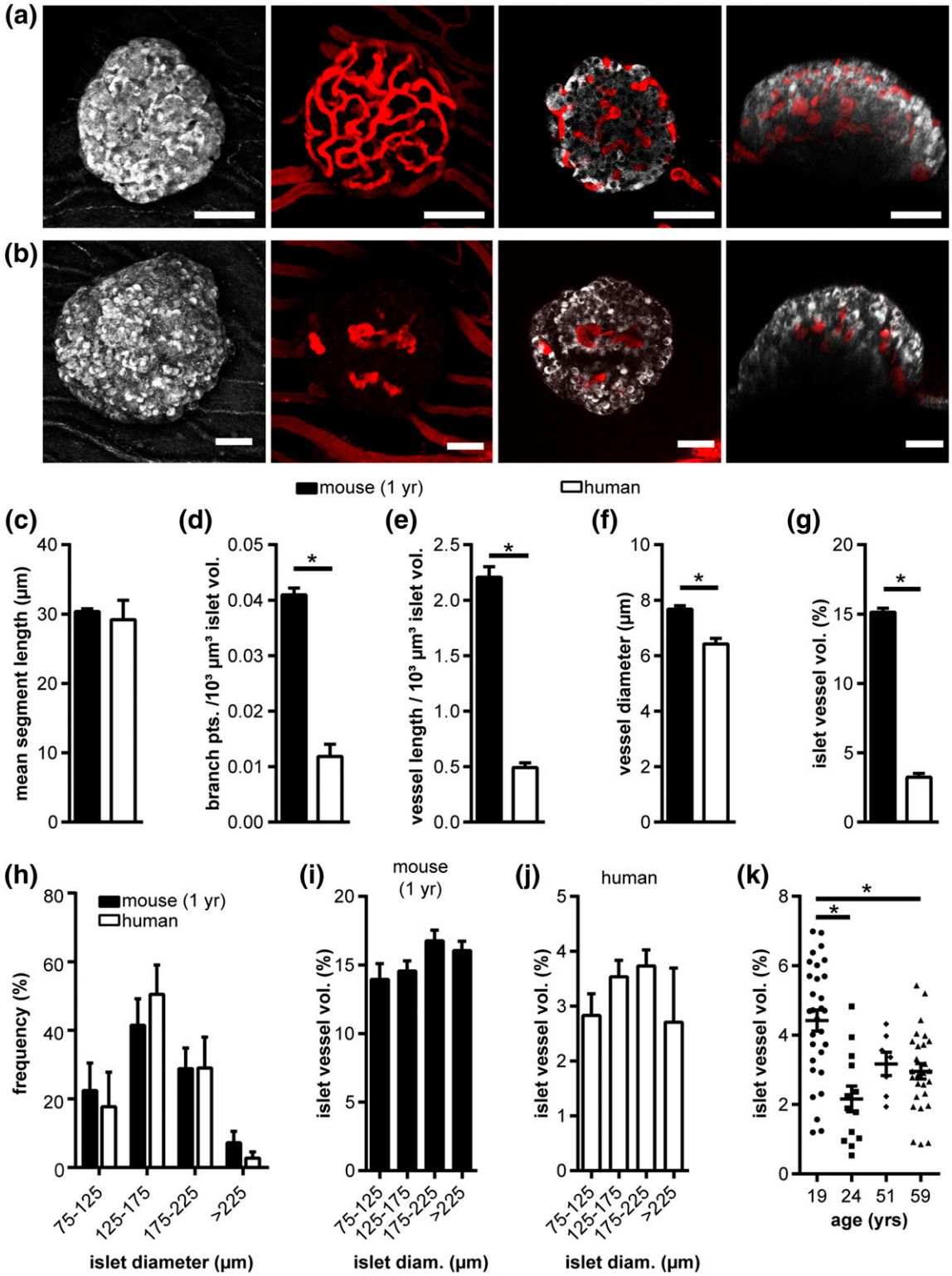

Figure 3. Vascular network of adult human and 1-year-old mouse islets after transplantation. (a) *In vivo* fluorescence images of a mouse and (b) human islet engrafted in the AC of a mouse. Images show MIPs of backscatter light (gray) and vessels (red), as well as selected XY and XZ image planes. (c–g) Vessel network analysis of transplanted mouse and human islets *in vivo*, showing (c) mean segment vessel length, (d) normalized number of branch points, (e) normalized vessel length, (f) vessel diameter, and (g) islet vessel volume fraction. (h) Distribution of transplanted mouse and human islet size. (i,j) Islet vessel volume fraction grouped by islet size for (i) mouse and (j) human islets. (k) Human islet vessel volume fraction grouped by donor age. Values are given as mean ± SEM for 6 mice (n = 44 mouse islets; 7.3 ± 0.4 islets per mouse) and 13 mice (n = 77 human islets; 5.9 ± 0.6 islets per mouse). *$P < 0.05$. Scale bars = 50 µm. diam, diameter.

and human donor islets of similar diameter distribution were used for transplantation [Fig. 3(h)]. In addition, we observed no significant effect of islet size on the vascular fraction after revascularization in either species [Fig. 3(i) and 3(j)]. Interestingly, although islet vascular fraction was persistently lower in human islets, it differed significantly between some organ donor preparations [Fig. 3(k)].

Comparing the intraislet vascular network of endogenous pancreatic islets and islets after transplantation (Fig. 4) revealed that mouse islets from 1-year-old mice in the pancreas and after engraftment in the AC displayed markedly different properties of their vascular network, showing increased mean segment length and vessel diameter, as well as a decrease in branching and vessel length leading to a 27% decrease in vessel fraction [Fig. 4(a–e)]. Similarly, but even more pronounced, transplanted human islets exhibited a strongly altered vascular network with significantly different branching, vessel length, vessel diameter, and a 64% reduced vessel fraction [Fig. 4(f–j)]. These results indicate that aged mouse islets and human islets show limited potential to fully recover their endogenous vessel network after transplantation.

Potential to rebuild the endogenous islet vessel network after transplantation was affected by donor islet age rather than a xenogeneic environment

Because islets of the youngest human donor showed the highest intraislet vascular fraction after transplantation, we assessed the effect of age on mouse islet revascularization by comparing engraftment of islets from 1-year and 12-week-old donors in hosts of identical age. *In situ*, endogenous pancreatic islets of 12-week-old mice [Fig. 5(a)] showed a less elaborate vascular network in comparison with endogenous islets of 1-year-old mice, with significant differences in mean segment length, branch points, and vessel length, diameter, and fraction [Fig. 5(b–f)]. However, after transplantation, islets from 12-week-old mice not only reestablished their endogenous network but exhibited an increased

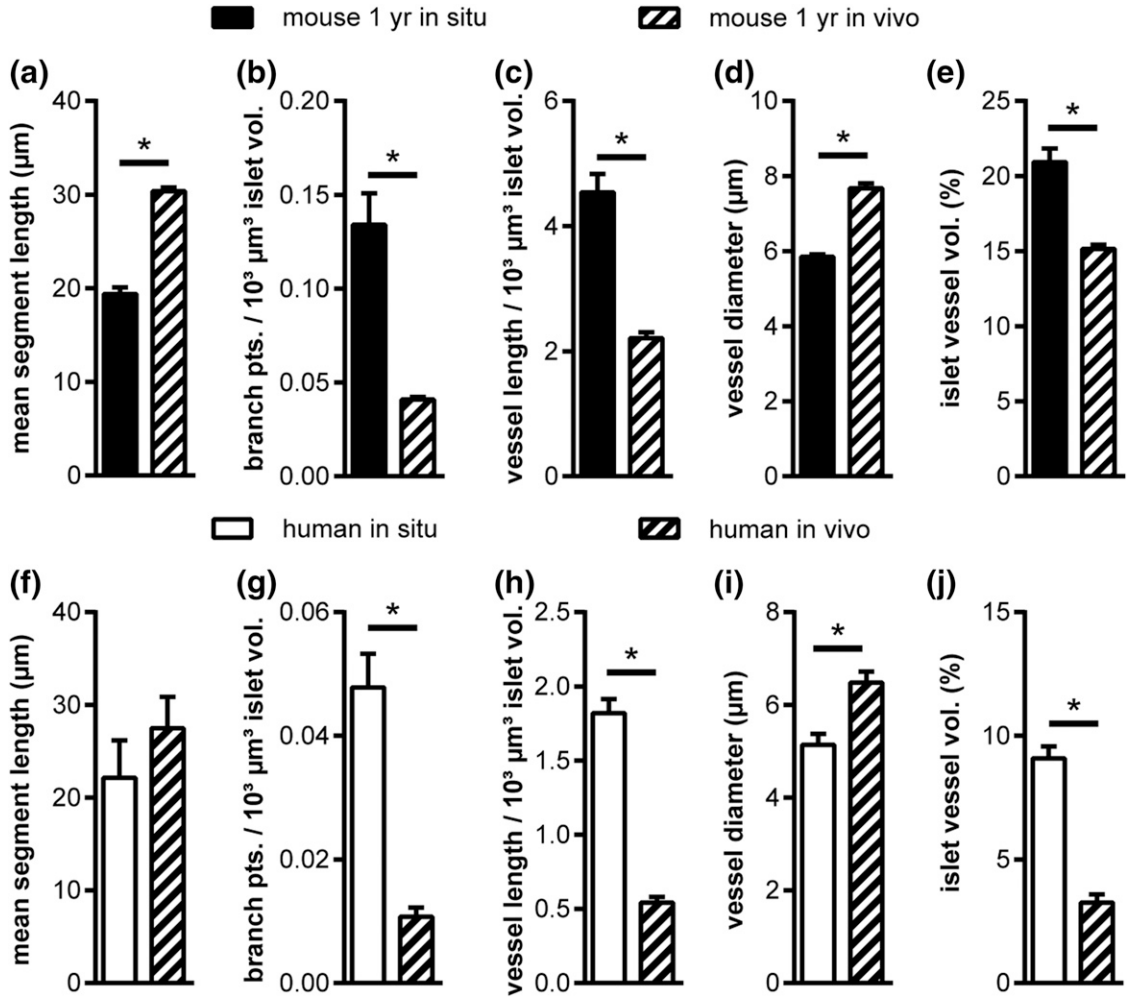

Figure 4. Comparison of 1-year-old mouse and adult human islet vascular network *in situ* and after transplantation *in vivo*. (a–j) Vascular network parameters *in situ* and after transplantation into the AC of mice *in vivo* for (a–e) mouse and (f–j) human islets. Values are given as mean ± SEM. $*P < 0.05$.

mean segment length and vascular fraction after revascularization [Fig. 5(g–l)], suggesting that islet donor age has an effect on revascularization potential after transplantation.

Finally, we evaluated if the potential of human and mouse islets to revascularize after transplantation in the AC of mice could also be affected by the xenogenic vs allogenic environment. Therefore, we studied the ability of porcine islets to rebuild their intraislet vascular network after engraftment in mice (Fig. 6). Our data revealed that endogenous porcine islets exhibit vessel network parameters similar to human islets in pancreas tissue slices *in situ* [Fig. 6(a) and 6(c–g)]. Strikingly, porcine donor islets isolated from young, 6- to 18-month-old, pigs reestablished their endogenous vascular network after transplantation into the AC of mice, with no significant changes in mean segment length, branch points, total vessel network length, vessel diameter, or fractional vessel volume [Fig. 6(b) and 6(c–g)]. However, porcine donor islets from more mature 3- to 5-year-old pigs were not able to rebuild their endogenous vascular network after transplantation [Fig. 6(c–g)], showing a decrease in branch points, total vessel network length, and fractional vessel volume comparable to engrafted human islets (Fig. 4). Identical to transplanted human and aged mouse islets, vessel diameter in old porcine islets was increased after transplantation [Fig. 6(f)]. These data further demonstrate that islet donor age, rather than the xenogeneic environment, contributed to the reduced islet revascularization after transplantation of mature human and porcine islets.

Discussion

In this study, we determined the unperturbed 3D arrangement of endocrine cells and vascular network of human islets *in situ*. To that aim, we used fresh pancreatic tissue originating from patients undergoing partial pancreatectomy because of a pancreatic tumor. The tissue used in our study displayed no signs of tumorous cells or fibrosis. Nevertheless, a potential effect of the tumor on islets in the neighboring healthy tissue by circulating factors cannot be fully excluded and might influence the results of our study. This, however, seems unlikely; despite different histopathology and type of pancreatic tumor removed, we found endocrine and vascular islet parameters in the studied healthy tissue to be similar between donors. In addition, a recent study by Ehehalt *et al.* (24) on glucose homeostasis of patients undergoing partial pancreatectomy reported that longstanding diabetes is typically not corrected by removal of the pancreatic tumor. Furthermore, the authors showed that recent-onset diabetes in patients with pancreatic cancer was often secondary to increased liver insulin resistance induced by the tumor and was resolved after tumor removal and improvement of insulin resistance. Strikingly, insulin levels were elevated in presence of the tumor, most likely in an attempt to compensate for increased insulin resistance, and these normalized after removal of the tumor. These observations indicate that islets in the healthy tissue of the pancreas are not affected by the pancreatic tumor. Therefore, in combination with the pancreas-tissue slice technique (3, 14–16, 25), this approach currently reflects the only way to study unperturbed human islets of metabolically characterized subjects *in situ*.

Our results provide evidence that human islets show a substantially different vessel network architecture compared with mouse islets. In addition to the recently observed reduced vessel-per-islet area in histological sections (26) our 3D analysis demonstrated that human islets exhibit a smaller vessel diameter as well as a less complex and shorter vessel network. We furthermore show that the vascular network in human islets is encompassed by α cells and that a large fraction of β cells is in a second and even third cell layer away from endothelial cells. These results support the model of an organized cellular architecture within human islets (8). In addition, however, our data suggest that due to islet vessel network architecture and spatial cell arrangement, a significant number of human β cells are not in direct contact with a blood vessel. In contrast, in mouse (this study) and rat (27) islets, almost all β cells are located next to vessels. This direct contact of endocrine and endothelial cells was suggested to be important in modulating islet cell function (5, 6). However, a twofold reduction of mouse islet vascularization did not lead to any change in β-cell gene expression or function (28). Thus, the exact role of endothelial cell input on islet cell function remains unclear. Moreover, our findings indicate that in human islets, not all β cells require endothelial cell input to assure appropriate functionality.

Another important modulator of islet function is the paracrine and juxtracrine cross-talk of endocrine cell types within the islet (1). Our analysis shows that in human islets, the vast majority of β cells have direct contact to neighboring α and β cells. This arrangement allows close bidirectional interaction and paracrine signaling of α and β cells independent of islet blood flow pattern and islet size. Additionally, our study shows that the specific architecture of human islets leads to the formation of independent β-cell clusters within islets, explaining different patterns of β-cell synchronicity observed in mouse and human islets (29). Therefore, the described morphological differences favor a diverse intraislet regulation of hormone secretion in mouse and human islets.

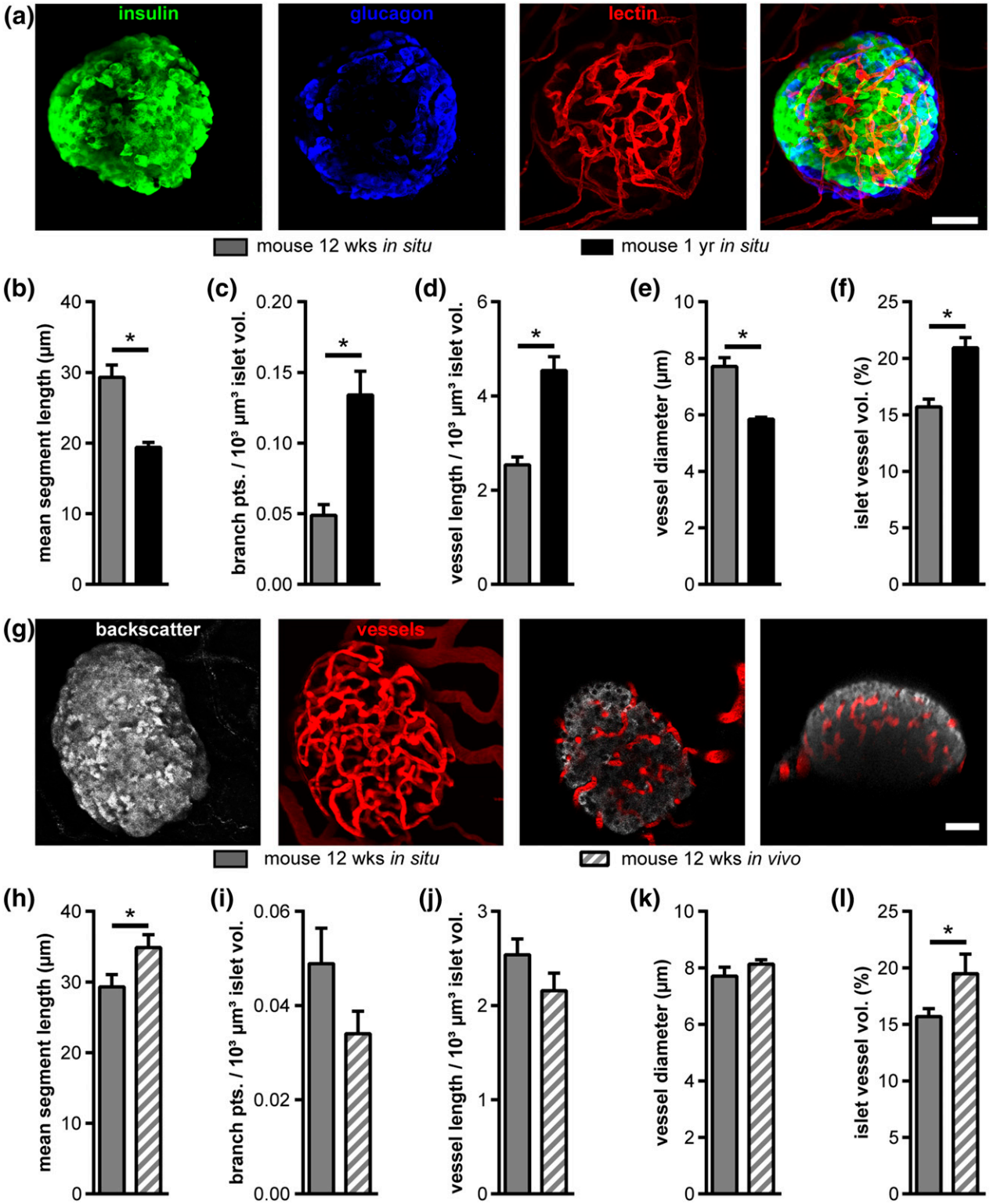

Figure 5. Effect of age on mouse islet vascularization *in situ* and *in vivo*. (a) Fluorescence images of a mouse islet within pancreas tissue slices from a 12-week-old mouse. Images show MIPs of staining for insulin (green), glucagon (blue), and blood vessels (red), as well as a merged MIP. (b–f) Comparison of vascular network parameters of islets from young (12 weeks) and aged (1 year) mice *in situ*: (b) mean vessel segment length, (c) normalized number of branch points, (d) normalized vessel length, (e) mean vessel diameter, and (f) mean islet vessel volume fraction. (g) *In vivo* fluorescence images of a mouse islet (12-week-old donor mouse) engrafted in the AC of a mouse. Images show MIPs of backscatter light (gray) and vessels (red), as well as selected XY and XZ image planes. (h–l) Comparison of vessel networks of young mouse islets *in situ* and after transplantation into the AC of mice *in vivo*, showing (h) mean segment vessel length, (i) normalized number of branch points, (j) normalized vessel length, (k) vessel diameter, and (l) islet vessel volume fraction. Values are given as mean ± SEM for (b–f) 9 mice (n = 74 islets; 8.2 ± 0.8 islets per mouse) at the age of 12 weeks and 10 mice (n = 97 islets; 9.7 ± 0.7 islets per mouse) at the age of 1 year *in situ*; (h–l) 6 mice (n = 35 islets; 5.8 ± 0.8 islets per mouse) for 12-week-old donors and 6 mice (n = 44 mouse islets; 7.3 ± 0.4 islets per mouse) for 1-year-old donors *in vivo*. *$P < 0.05$. Scale bars = 30 µm (a) and 50 µm (g).

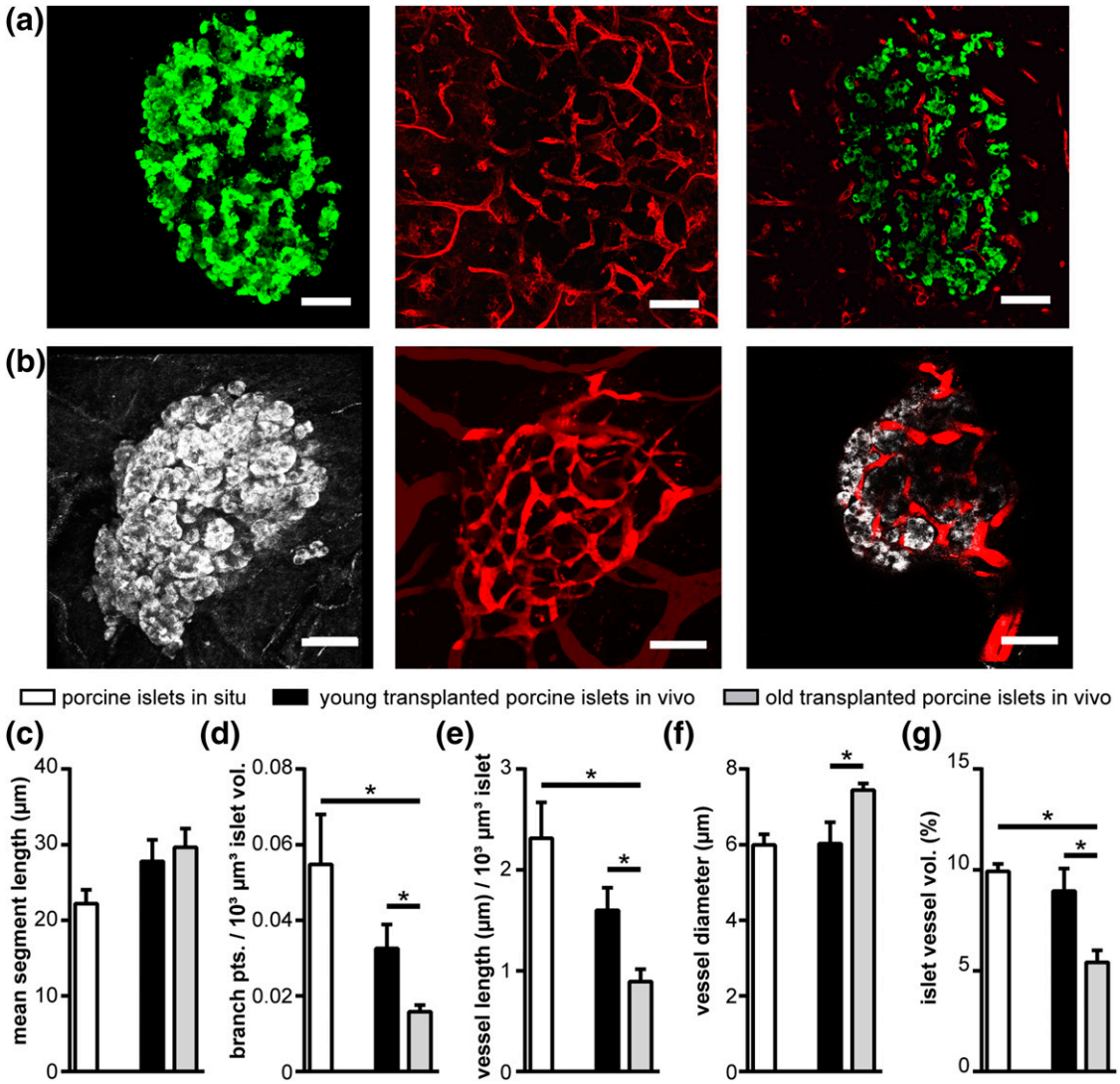

Figure 6. Vascularization of porcine islets *in situ* and after transplantation with different islet donor ages. (a,b) Images of (a) porcine islets *in situ* and (b) after transplantation to the AC of mice *in vivo*. Images show MIPs of insulin (green) or backscatter light (gray) and vessels (red), as well as a selected XY image plane. (c–g) Vessel network analysis of porcine islets *in situ* and after transplantation of young (6 to 18 months) and old (3 to 5 years) porcine donor islets to the AC of mice *in vivo*, showing (c) mean segment vessel length, (d) normalized number of branch points, (e) normalized vessel length, (f) vessel diameter, and (g) islet vessel volume fraction. Values are given as mean ± SEM for 3 pigs (n = 27 islets; 9.0 ± 0.6 islets per pig) *in situ*, 6 mice for young porcine islet donors (n = 24 transplanted islets; 4.0 ± 1.0 islets per mouse), and 8 mice for old porcine islet donors (n = 33 transplanted islets; 4.1 ± 0.6 islets per mouse). *$P < 0.05$. Scale bars = 50 µm.

In combination with the *in situ* analyses, we aimed to investigate if islets after transplantation have the capability to rebuild their endogenous vascular network, because inadequate revascularization is believed to contribute to reduced graft survival after islet transplantation (30). Our results show that islets from aged mice display a reduced potential to rebuild their endogenous vascular network during engraftment and that this effect is further pronounced in adult human islets transplanted into the same site. This observation is in line with previous reports showing decreased vessel density in mouse and human islets upon transplantation (31–34), and this effect will potentially result in long-term deterioration of islet cell function and mass, due to a relative lack in oxygen and nutrient supply. However, our study also demonstrates that islets from young mice are able to rebuild their full endogenous vessel network with an even enlarged islet vascular fraction, indicating a donor age-dependent effect on islet revascularization after transplantation. Likewise, islets from the youngest human donor in our study showed the highest vascular fraction after transplantation. Nonetheless, there is no clear correlation with age across all donors, probably because many additional factors, like donor health status, cause of death, or isolation procedure, will contribute to a different quality of isolated human islets and their engraftment capability, masking a possible age effect. Yet, a donor age-dependent decrease in blood flow has been previously observed in human islets transplanted under the

mouse kidney capsule, but could not be correlated to decreased vascular density in the islets (33) and thereby might be related to additional vessel network parameters. Exploring the presence of a donor-age effect on revascularization of transplanted human islets similar to that observed with mouse islets would require the availability of adolescent human donor islets, which was not possible during this study.

Nevertheless, we could further corroborate the donor age-dependent potential of islet revascularization by transplanting porcine islets, which exhibit a very similar vascular network to human islets *in situ*. Whereas old porcine donor islets displayed the same vascular network alterations as human islets after transplantation, young porcine donor islets were able to fully re-establish their endogenous vascular network. The equal handling of young and old porcine donor islets demonstrated that different revascularization capabilities occurred independently of diverse culture times before transplantation. This is in line with a recent report that used the same *in vivo* platform and found no effect of culture time on full islet revascularization (35). At the same time, these results mitigate the xenogeneic environment as reason for the further reduced revascularization observed for human islets and emphasize an islet donor-age effect. A potential limitation of our study is the limited number of islets and donors investigated. This is related to the complex experimental approaches, image acquisition, and analysis necessary to obtain this detailed insight into cellular morphology *in situ* and *in vivo*. Nevertheless, the low heterogeneity of our data between islets and donors suggest these findings reflect common features for the experimental settings applied in our study.

In summary, using a 3D approach, we have shown the detailed vascular network and cell architecture of unperturbed human islets *in situ* and after transplantation *in vivo*. Our study reveals that the distinct vascular network and endocrine cell arrangements of human islets limits β to endothelial cell contact, favors α–β cell interaction, and leads to distinct β-cell clusters within islets, all with potentially important consequences for juxtacrine and paracrine signaling in human islets. Furthermore, our data indicate that due to an age-dependent effect, adult human donor islets do not allow appropriate engraftment after transplantation; thus, induced enhancement of revascularization in adult human donor islets or the use of alternative, less-mature islet cell sources is proposed.

Acknowledgments

We thank Katharina Hüttner, Alin Pfennig, Chrissy Kühn, and Angela Hartke for excellent technical assistance, and Daniela Richter, Manuela Kleeberg, Florian Ehehalt, Marius Distler, Robert Grutzmann, and Gustavo Baretton for provision of human pancreatic tissues.

Address all correspondence and requests for reprints to: Stephan Speier, PhD, Paul Langerhans Institute Dresden, Tatzberg 47/49, 01307 Dresden, Germany. E-mail: stephan.speier@tu-dresden.de.

This work was supported by the Emmy Noether Program of the German Research Foundation (DFG; www.dfg.de); the CRTD–DFG Research Center for Regenerative Therapies Dresden, Cluster of Excellence (www.crt-dresden.de); the DFG-SFB/Transregio 127; the German Ministry for Education and Research (www.bmbf.de) to the German Centre for Diabetes Research and to the Network of Competence for Diabetes; and the European Foundation for the Study of Diabetes/Boehringer Ingelheim Basic Research Program. The work leading to this publication has received support from the Innovative Medicines Initiative Joint Undertaking under grant agreement no. 155005 (IMIDIA), resources of which are composed of financial contributions from the European Union's Seventh Framework Program (FP7/2007-2013) and European Federation of Pharmaceutical Industries and Associations companies' in kind contribution.

Author contributions: C.M.C., C.C., and S.S. conceived and designed the experiments, and prepared the manuscript; C.C. and S.R.J. performed all mouse experiments and analyzed data. C.M.C. and J.S. performed all human and porcine experiments and analyzed data. H.C. analyzed data and provided intellectual input. A.B., N.K., and E.W. provided porcine tissue. A.S., B.L., and S.R.B. provided porcine islets. V.K. and S.R.B. provided human islets. J.W. and M.S. provided human tissue for *in situ* analyses. C.M.C., C.C., J.S., A.B., N.K., E.W., S.R.B., M.S., and S.S. prepared and/or revised the manuscript. S.S. is the guarantor of this work.

Disclosure Summary: The authors have nothing to disclose

References

1. Jain R, Lammert E. Cell-cell interactions in the endocrine pancreas. *Diabetes Obes Metab*. 2009;**11**(Suppl 4):159–167.
2. Ishihara H, Maechler P, Gjinovci A, Herrera PL, Wollheim CB. Islet beta-cell secretion determines glucagon release from neighbouring alpha-cells. *Nat Cell Biol*. 2003;**5**(4):330–335.
3. Speier S, Gjinovci A, Charollais A, Meda P, Rupnik M. Cx36-mediated coupling reduces beta-cell heterogeneity, confines the stimulating glucose concentration range, and affects insulin release kinetics. *Diabetes*. 2007;**56**(4):1078–1086.
4. Schuit FC, Derde MP, Pipeleers DG. Sensitivity of rat pancreatic A and B cells to somatostatin. *Diabetologia*. 1989;**32**(3):207–212.
5. Konstantinova I, Nikolova G, Ohara-Imaizumi M, Meda P, Kucera T, Zarbalis K, Wurst W, Nagamatsu S, Lammert E. EphA-Ephrin-A-mediated beta cell communication regulates insulin secretion from pancreatic islets. *Cell*. 2007;**129**(2):359–370.
6. Nikolova G, Jabs N, Konstantinova I, Domogatskaya A, Tryggvason K, Sorokin L, Fässler R, Gu G, Gerber HP, Ferrara N, Melton DA, Lammert E. The vascular basement membrane: a niche for insulin gene expression and beta cell proliferation. *Dev Cell*. 2006;**10**(3):397–405.
7. Brunicardi FC, Stagner J, Bonner-Weir S, Wayland H, Kleinman R, Livingston E, Guth P, Menger M, McCuskey R, Intaglietta M, Charles A, Ashley S, Cheung A, Ipp E, Gilman S, Howard T, Passaro E, Jr; Long Beach Veterans Administration Regional Medical Education Center Symposium. Microcirculation of the islets of Langerhans. *Diabetes*. 1996;**45**(4):385–392.

8. Bosco D, Armanet M, Morel P, Niclauss N, Sgroi A, Muller YD, Giovannoni L, Parnaud G, Berney T. Unique arrangement of alpha- and beta-cells in human islets of Langerhans. *Diabetes*. 2010;**59**(5): 1202–1210.
9. Kim A, Miller K, Jo J, Kilimnik G, Wojcik P, Hara M. Islet architecture: a comparative study. *Islets*. 2009;**1**(2):129–136.
10. Hoang DT, Matsunari H, Nagaya M, Nagashima H, Millis JM, Witkowski P, Periwal V, Hara M, Jo J. A conserved rule for pancreatic islet organization. *PLoS One*. 2014;**9**(10):e110384.
11. Arrojo e Drigo R, Ali Y, Diez J, Srinivasan DK, Berggren PO, Boehm BO. New insights into the architecture of the islet of Langerhans: a focused cross-species assessment. Diabetologia 2015;58(10):2218–2228.
12. Bonner-Weir S, Sullivan BA, Weir GC. Human islet morphology revisited: human and rodent islets are not so different after all. J Histochem Cytochem. 2015;63:604-612.
13. Murakami T, Fujita T, Taguchi T, Nonaka Y, Orita K. The blood vascular bed of the human pancreas, with special reference to the insulo-acinar portal system. Scanning electron microscopy of corrosion casts. *Arch Histol Cytol*. 1992;**55**(4):381–395.
14. Marciniak A, Cohrs CM, Tsata V, Chouinard JA, Selck C, Stertmann J, Reichelt S, Rose T, Ehehalt F, Weitz J, Solimena M, Slak Rupnik M, Speier S. Using pancreas tissue slices for in situ studies of islet of Langerhans and acinar cell biology. *Nat Protoc*. 2014;**9**(12): 2809–2822.
15. Marciniak A, Selck C, Friedrich B, Speier S. Mouse pancreas tissue slice culture facilitates long-term studies of exocrine and endocrine cell physiology in situ. *PLoS One*. 2013;**8**(11):e78706.
16. Speier S, Rupnik M. A novel approach to in situ characterization of pancreatic beta-cells. *Pflugers Arch*. 2003;**446**(5):553–558.
17. Chmelova H, Cohrs CM, Chouinard JA, Petzold C, Kuhn M, Chen C, Roeder I, Kretschmer K, Speier S. Distinct roles of β-cell mass and function during type 1 diabetes onset and remission. *Diabetes*. 2015;**64**(6):2148–2160.
18. Ricordi C, Socci C, Davalli AM, Staudacher C, Vertova A, Baro P, Sassi I, Braghi S, Guizzi N, Pozza G, Di Carlo V. Application of the automated method to islet isolation in swine. *Transplant Proc*. 1990;**22**(2):784–785.
19. Virtanen I, Banerjee M, Palgi J, Korsgren O, Lukinius A, Thornell LE, Kikkawa Y, Sekiguchi K, Hukkanen M, Konttinen YT, Otonkoski T. Blood vessels of human islets of Langerhans are surrounded by a double basement membrane. *Diabetologia*. 2008; **51**(7):1181–1191.
20. Speier S, Nyqvist D, Cabrera O, Yu J, Molano RD, Pileggi A, Moede T, Köhler M, Wilbertz J, Leibiger B, Ricordi C, Leibiger IB, Caicedo A, Berggren PO. Noninvasive in vivo imaging of pancreatic islet cell biology. *Nat Med*. 2008;**14**(5):574–578.
21. Speier S, Nyqvist D, Köhler M, Caicedo A, Leibiger IB, Berggren PO. Noninvasive high-resolution in vivo imaging of cell biology in the anterior chamber of the mouse eye. *Nat Protoc*. 2008;**3**(8): 1278–1286.
22. Kilimnik G, Zhao B, Jo J, Periwal V, Witkowski P, Misawa R, Hara M. Altered islet composition and disproportionate loss of large islets in patients with type 2 diabetes. *PLoS One*. 2011;**6**(11):e27445.
23. Kilimnik G, Jo J, Periwal V, Zielinski MC, Hara M. Quantification of islet size and architecture. *Islets*. 2012;**4**(2):167–172.
24. Ehehalt F, Sturm D, Rösler M, Distler M, Weitz J, Kersting S, Ludwig B, Schwanebeck U, Saeger HD, Solimena M, Grützmann R. Blood glucose homeostasis in the course of partial pancreatectomy–evidence for surgically reversible diabetes induced by cholestasis. *PLoS One*. 2015;**10**(8):e0134140.
25. Speier S, Yang SB, Sroka K, Rose T, Rupnik M. KATP-channels in beta-cells in tissue slices are directly modulated by millimolar ATP. *Mol Cell Endocrinol*. 2005;**230**(1-2):51–58.
26. Brissova M, Shostak A, Fligner CL, Revetta FL, Washington MK, Powers AC, Hull RL. Human Islets have fewer blood vessels than mouse islets and the density of islet vascular structures is increased in type 2 diabetes. *J Histochem Cytochem*. 2015;**63**:637–645.
27. Bonner-Weir S. Morphological evidence for pancreatic polarity of beta-cell within islets of Langerhans. *Diabetes*. 1988;**37**(5): 616–621.
28. Reinert RB, Brissova M, Shostak A, Pan FC, Poffenberger G, Cai Q, Hundemer GL, Kantz J, Thompson CS, Dai C, McGuinness OP, Powers AC. Vascular endothelial growth factor-a and islet vascularization are necessary in developing, but not adult, pancreatic islets. *Diabetes*. 2013;**62**(12):4154–4164.
29. Quesada I, Todorova MG, Alonso-Magdalena P, Beltrá M, Carneiro EM, Martin F, Nadal A, Soria B. Glucose induces opposite intracellular Ca2+ concentration oscillatory patterns in identified alpha- and beta-cells within intact human islets of Langerhans. *Diabetes*. 2006;**55**(9):2463–2469.
30. Pepper AR, Gala-Lopez B, Ziff O, Shapiro AM. Revascularization of transplanted pancreatic islets and role of the transplantation site. *Clin Dev Immunol*. 2013;**2013**:352315.
31. Mattsson G, Jansson L, Carlsson PO. Decreased vascular density in mouse pancreatic islets after transplantation. *Diabetes*. 2002;**51**(5): 1362–1366.
32. Olsson R, Olerud J, Pettersson U, Carlsson PO. Increased numbers of low-oxygenated pancreatic islets after intraportal islet transplantation. *Diabetes*. 2011;**60**(9):2350–2353.
33. Carlsson PO, Palm F, Mattsson G. Low revascularization of experimentally transplanted human pancreatic islets. *J Clin Endocrinol Metab*. 2002;**87**(12):5418–5423.
34. Liljeback H, Grapensparr L, Olerud J, Carlsson PO. Extensive loss of islet mass beyond the first day after intraportal human islet transplantation in a mouse model. *Cell Transplant*. 2016;**25**(3): 481–489.
35. Nyqvist D, Speier S, Rodriguez-Diaz R, Molano RD, Lipovsek S, Rupnik M, Dicker A, Ilegems E, Zahr-Akrawi E, Molina J, Lopez-Cabeza M, Villate S, Abdulreda MH, Ricordi C, Caicedo A, Pileggi A, Berggren PO. Donor islet endothelial cells in pancreatic islet revascularization. *Diabetes*. 2011;**60**(10):2571–2577.